Boiling of Small Droplets

M. L. Roesle and F. A. Kulacki

Department of Mechanical Engineering, University of Minnesota, 111 Church St. S.E. Minneapolis, MN 55455, United States

Abstract

Analysis is reported of the boiling of small diameter suspended droplets, such as found in emulsions. A one-dimensional model considers both the energy and momentum equations, and effects of differences in fluid and thermodynamic properties between the droplet and the surrounding liquid are examined. Results are presented in the form of time varying bubble radius and temperature. The initial boiling of the droplet is insensitive to the surrounding liquid and droplet diameter, while the final evaporation rate is strongly affected by the properties of the surrounding liquid. After a droplet has completely evaporated, the vapor bubble expands and contracts via radial oscillations near the Minnaert frequency for isothermal bubbles. Thermal damping is observed but the model does not capture acoustic damping.

Keywords: Boiling, emulsion, droplet

Nomenclature

c	Liquid specific heat, kJ/kg-°C
c_v	Vapor constant volume specific heat, kJ/kg-°C
d	Diameter, m
F	Source flow strength, m^3/s
f_M	Minnaert frequency, Eq. (14)
h	Heat transfer coefficient, W/m^2-°C
i	Specific enthalpy, J/kg
Ja	Jakob number, $\rho_f c_f \Delta T/(\rho_g i_{fg})$
k	Thermal conductivity, W/m-°C
m	Mass, kg
N	Number of nodes
Nu	Nusselt number, hd_b/k

P	Pressure, N/m^2
Pe	Péclet number, RePr
Pr	Prandtl number, ν/α
R	Droplet or bubble radius, m
R^+	Nondimensional bubble radius, Eq. (1b)
R_{cr}	Critical bubble radius, Eq. (3)
R_s	Specific gas constant, kJ/kg-K
r	Radial distance, m
Re	Reynolds number, Ud_d/ν
T	Temperature, K
ΔT	Overall driving temperature difference, $T_\infty - T_{sat}(P_\infty)$
t	Time, s
t^+	Nondimensional time, Eq. (1b)
U	Bubble velocity, m/s
u	Radial velocity, m/s

Greek Symbols

α	Thermal diffusivity, m^2/s
γ	Vapor specific heat ratio
δ	Thermal boundary layer thickness, m
κ	Polytropic coefficient
ν	Kinematic viscosity, m^2/s
ρ	Density, kg/m^3
σ	Surface tension, N/m

Subscripts

0	Reference or equilibrium condition
b	Bubble
c	Carrier fluid surrounding the droplet
d	Droplet

f	Saturated liquid
fg	Difference between saturated vapor and saturated liquid
g	Saturated vapor
j	Counting index
sat	Saturated condition
v	Vapor phase
∞	Ambient condition

1. Introduction

The growth of vapor bubbles suspended in liquid has been the subject of study for several decades. Early studies examined the expansion of vapor bubbles in uniformly superheated liquid. In these studies the bubble is generally assumed to be stationary in the surrounding liquid and spherical. Expansion of the bubble is initially limited by the inertia of the surrounding liquid and later by thermal diffusion to the bubble surface [1]. More recently boiling in suspended droplets has received increasing attention. Typically the droplets under study have d ~ 1 mm, as are found in direct contact heat exchangers. Buoyancy becomes important in these cases because the evaporating droplet hangs on the bottom of the growing vapor bubble and the rate of boiling is determined by convection to the bubble-droplet pair as they rise through the surrounding liquid [2].

Recent studies of boiling dilute emulsions have identified unusual boiling behavior attributed to the boiling of individual droplets while in suspension [3]. These droplets are typically two to three orders of magnitude smaller than those found in direct contact heat exchangers, and so their behavior during boiling is also quite different. Such small droplets have insignificant drift velocity and boil so quickly that gravitational effects are negligible. Inertial effects are significant however, and the heat transfer properties of the liquid around the droplet are important in the later stages of boiling. The behavior of the bubble after the droplet has completely evaporated also merits examination. A better understanding of how boiling occurs in such small droplets is important to understanding the overall behavior of a boiling dilute emulsion.

Because studies of boiling droplets for direct contact heat exchangers generally do not address these issues, a numerical study is performed of boiling in very small suspended droplets with nucleation inside the droplet. A one-dimensional model of a boiling droplet that includes both the momentum and thermal energy equations is developed, and a series of simulations are presented for conditions typical of those reported in the boiling emulsion literature. For the present study, we restrict the model to small droplets with moderate levels of superheat in the surrounding fluid.

2. Prior Work

The growth of vapor bubbles in a superheated liquid is a complicated phenomenon and involves the effects of thermal diffusion and inertia in the surrounding liquid and surface tension at the surface of the bubble. Different effects are dominant at different times and under different conditions, and accurate modeling of all stages of bubble growth has only been accomplished with numerical simulation. Boiling of suspended droplets is more complex still, as buoyancy causes the droplet and bubble to move through the surrounding liquid and lose spherical symmetry.

Generally, a vapor bubble that forms in superheated liquid undergoes three phases of growth. The bubble starts with the same temperature as the surrounding liquid and its growth is driven by the difference between the vapor pressure inside the bubble and the ambient pressure. This driving pressure difference is initially nearly balanced by the surface tension of the bubble and the bubble experiences surface tension dominated growth. The pressure jump due to surface tension varies with the inverse of the bubble diameter so that the effect of surface tension quickly becomes negligible as the bubble size increases. When surface tension becomes negligible the bubble enters inertia dominated growth where the rate of growth is limited by the inertia of the surrounding liquid (Fig 1a). As the bubble continues to expand, evaporation at the surface causes its temperature to decrease, and the vapor pressure inside the bubble decreases until eventually there is zero driving force due to pressure difference. At this point the bubble enters thermal diffusion dominated growth (Fig 1b). For a bubble growing in uniformly-superheated liquid, this phase of growth continues indefinitely [4].

An analytical solution for the growth of vapor bubbles in superheated liquid, valid in both the inertia and thermal diffusion dominated phases, is developed by Mikic et al. [1] They find a set of scaled coordinates,

$$R^+ = \frac{\pi}{12}\sqrt{\frac{2i_{fg}\rho_v\Delta T}{3\rho_f T_{sat}}}\,\frac{R}{Ja^2\alpha_f}, \tag{1a}$$

$$t^+ = \frac{\pi}{18}\,\frac{i_{fg}\rho_v\Delta T}{\rho_f T_{sat}}\,\frac{t}{Ja^2\alpha_f}, \tag{1b}$$

for which bubble growth collapses to a single curve,

$$R^+ = \frac{2}{3}\left[\left(t^+ + 1\right)^{3/2} - \left(t^+\right)^{3/2} - 1\right]. \tag{2}$$

Like most analytical approaches, this solution neglects surface tension. For large t^+, $R^+ \sim (t^+)^{1/2}$, which matches the analysis of Plesset and Zwick [5] for thermal diffusion dominated growth. At small t^+, $R^+ \sim t^+$, which is similar to the Rayleigh solution for inertia dominated growth [6]. Unlike the Rayleigh solution, Eqs. (1a,b) do not contain a driving pressure difference. Instead, the pressure difference is replaced by a driving temperature difference, ΔT, through the use of a linearized version of the Clausius-Clapeyron equation. This approximation can introduce errors for large superheat [7], but Eq. (2) is found to agree well with experimental data for moderate superheat [8].

Analytical solutions are generally not possible when more accurate models of either fluid properties or the thermal boundary layer are utilized. The numerical study of Lee and Merte [4] uses accurate models of fluid properties and simulates the temperature field surrounding the bubble. They also include the surface tension of the bubble and begin the simulation with a bubble radius very close to the critical radius, R_{cr}, where,

$$R_{cr} = \frac{2\sigma}{P_{sat}(T_\infty) - P_\infty}. \tag{3}$$

Because a bubble at the critical radius is in unstable equilibrium, a small perturbation in the radius is required to cause the bubble to expand. Lee and Merte show that for small perturbations, the magnitude of the perturbation has no effect on the subsequent expansion of the bubble aside from a change in the time that elapses before the bubble begins to expand rapidly. Their simulations show good agreement with experimental studies for a wide range of fluids, ambient pressures, and degrees of superheat. They also find that the

model of Mikic et al. [1] is accurate in many cases except for the very earliest stage of bubble growth where surface tension plays a significant role.

These studies of bubbles in uniformly superheated liquid have limited applicability to suspended droplets because they do not consider the interaction between the bubble, droplet, and the surrounding liquid, as well as the loss of spherical symmetry that occurs due to buoyancy. Sideman and Taitel [2] study evaporating droplets of superheated pentane and butane with $1.9 < d_d < 3.9$ mm and develop an analytical model that predicts a relation between the Nusselt and the Péclet numbers of the evaporating droplet. They assume that the bubble is spherical with the droplet forming a layer around the bottom portion of the bubble and steady potential flow around the bubble and droplet as they rise due to buoyancy. They find the rate of heat transfer to the droplet and compare it to experimental results obtained by photographing droplets boiling while rising through water. Tochitani and co-workers [9,10] also develop an analytical model of heat transfer to a boiling droplet using a geometric model of the droplet similar to that of Sideman and Taitel, but assume that the flow around the droplet is Stokes flow rather than potential flow. They also find a relationship between the Nusselt and the Péclet numbers and find that it matches experimental results for $0.8 < d_d < 1.4$ mm and $Re < 1$. Battya, Raghavan, and Seetharamu [11] re-examine the data of Sideman and Taitel and find that the Nusselt number also depends on the Jakob number. The correlations of Sideman and Taitel, Tochitani et al., and Battya et al. all predict that $Nu \rightarrow 0$ as $Pe \rightarrow 0$, and thus none of them are appropriate for very small droplets that have negligible velocity relative to that of the surrounding liquid.

Other researchers examine boiling droplets using more sophisticated models of the geometry of the bubble and droplet [12,13]. Raina and Grover [14] study the effects of sloshing of the droplet around the bubble. Mahoud [15] performs numerical simulations of boiling droplets in which the bubble and droplet are concentric, and Wohak and Beer [16] perform axisymmetric simulations of a boiling deformable droplet. All of these studies examine droplets with $d_d \sim 1$ mm that boil in time scales of milliseconds to seconds. Therefore they are concerned with a different set of processes and forces than are dominant in boiling of very small droplets.

Avedisian [17] studies several aspects of boiling superheated droplets including droplets at rest in the surrounding liquid. For such stationary droplets he adopts a one-dimensional model, assuming that the growing vapor bubble is close to the center of the droplet. His model includes both momentum and energy balances, as well as surface tension, and thus his simulations predict all three phases of bubble growth. Avedisian applies a coordinate transformation that fixes the locations of the bubble and droplet, which simplifies his numerical solutions. He performs several simulations for droplets of moderate size, generally using the properties of n-octane boiling at its superheat limit, and the conditions are such that the bubble experiences inertia dominated growth only while the bubble is very small compared to the droplet size. He finds that the liquid around the droplet influences evaporation rate only during the final stages of boiling, when the thermal boundary layer around the bubble grows into the liquid surrounding the droplet. He finds that for $k_c/k_d > 1$ and $\alpha_c/\alpha_d < 1$ the late bubble growth accelerates, while it is hindered for $k_c/k_d < 1$ and $\alpha_c/\alpha_d > 1$. The coordinate transform used to fix the droplet and bubble surfaces requires that the simulations terminate when the droplet evaporates completely and thus the subsequent behavior of the bubble is not simulated.

Shepherd and Sturtevant [18] address rapid boiling of a superheated droplet. They observe boiling in droplets near their limit of superheat and compare the rate of expansion to the classical models of inertia dominated growth and thermal diffusion dominated growth for $0.5 < d_d < 1$ mm. They find that the vapor bubble grows more rapidly than predicted for thermal diffusion growth when the bubble reaches approximately the original size of the droplet. They attribute this deviation from theory to instabilities that roughen the bubble surface and thereby increase the surface area available for evaporation. They also observe oscillation of the resulting vapor bubble and instabilities that occur there as well. Thus, although this study observes bubble growth on a time scale close to that of droplets boiling in emulsions, it is principally concerned with instability that occurs at much larger length scales. Lee and Merte [19] and Frost and Sturtevant [20] also address instability of large boiling droplets near the superheat limit.

Kwak, Oh, and Park [21] study the oscillating bubble that results from a droplet boiling at its superheat limit. They develop coupled differential equations for the evolution over

time of the bubble pressure, temperature, radius and velocity, and the thickness of the thermal boundary layer:

$$\frac{dP_b}{dt} = -\frac{3\gamma P_b}{R_b}\frac{dR_b}{dt} - \frac{6(\gamma-1)k_c(T_b - T_\infty)}{\delta R_b}, \tag{4}$$

$$\frac{dT_b}{dt} = -\frac{3(\gamma-1)T_b}{R_b}\frac{dR_b}{dt} - \frac{6(\gamma-1)k_c T_b(T_b - T_\infty)}{\delta R_b P_b}, \tag{5}$$

$$R_b\frac{dU}{dt} + \frac{3}{2}U^2 = \frac{1}{\rho_c}(P_b - P_\infty), \tag{6}$$

$$U = \frac{dR_b}{dt}, \tag{7}$$

$$\left[1 + \frac{\delta}{R_b} + \frac{3}{10}\left(\frac{\delta}{R_b}\right)^2\right]\frac{d\delta}{dt} = \frac{6\alpha_c}{\delta} - \left[\frac{2\delta}{R_b} + \frac{1}{2}\left(\frac{\delta}{R_b}\right)^2\right]\frac{dR_b}{dt} - \delta\left[1 + \frac{\delta}{2R_b} + \frac{1}{10}\left(\frac{\delta}{R_b}\right)^2\right]\frac{1}{(T_b - T_\infty)}\frac{dT_b}{dt}. \tag{8}$$

They assume a quadratic temperature profile in the boundary layer. Because the last term of Eq. (8) contains the temperature difference $(T_b - T_\infty)$ in the denominator, they artificially set $d\delta/dt = 0$ when $|T_b - T_\infty| < 0.21°C$. This restriction ensures that the boundary layer thickness remains small compared to the bubble radius. They do not address in detail the boiling process that leads to the oscillating bubble. Park, Byun, and Kwak [22] compare this model to experimental results for droplets of different hydrocarbons with $d_d \sim 1$ mm boiling at their superheat limit and also develop a model for the pressure field far from the droplet during boiling. Park et al. add viscous and surface tension terms to Eq. (6), but for the size of the bubble they simulate, surface tension effects should generally be negligible.

3. Boiling Model

To gain an accurate picture of all stages of the boiling process in very small suspended droplets, a series of computer simulations are performed for various droplet sizes, degree of superheat, and combinations of fluid parameters for the droplet and surrounding liquid.

The modeling approach is similar to that of Avedisian [17], with the bubble-droplet system assumed to have spherical symmetry and both energy and momentum balances considered. The liquids are assumed to be incompressible and have constant properties, although the droplet and the surrounding liquid have different properties. The vapor in the bubble is assumed to obey the ideal gas law, and temperature and pressure are assumed to be uniform inside the vapor bubble. Unlike the work of Avedisian, we do not use a coordinate transform to fix the location of the bubble and droplet surfaces. Thus the present simulations can continue past the complete evaporation of the droplet.

The boiling process can be divided into two time domains based on the presence of droplet liquid. In the first time domain, the growth of the vapor bubble is accompanied by evaporation of the droplet liquid at the bubble surface. During this period the vapor in the bubble is assumed to be saturated, and the rate of evaporation of liquid at the droplet surface must be taken into account. The second time domain begins when the liquid has completely evaporated. During this period the mass of the vapor bubble remains constant and is no longer assumed to be saturated. The state of the vapor in the bubble is determined using the ideal gas law and the Clausius-Clapeyron equation.

3.1.Momentum balance

The liquid around the bubble is assumed to be incompressible, so continuity requires that the radial velocity be described by,

$$u(r,t)=\frac{F(t)}{r^2}. \tag{9}$$

Thus, if the velocity of the liquid can be found at any location at a given time, the entire velocity field in the liquid is known.

An equation for pressure is obtained by inserting Eq. (9) for velocity into the momentum equation,

$$\frac{\partial P}{\partial r}=\rho\left(\frac{2}{r}u^2-\frac{1}{r^2}\frac{dF(t)}{dt}\right). \tag{10}$$

Equation (10) can be integrated from the bubble surface out to infinity, where $P = P_\infty$. The result is given as Eq. (11), which also includes the pressure jump at the bubble surface due to surface tension. Surface tension at the droplet surface is neglected. At the beginning of the simulation, $R_b/R_d << 1$, so that the effect of surface tension at the droplet surface is negligible compared to surface tension at the bubble surface. After the droplet has completely evaporated, the resulting bubble has large enough radius so that the pressure jump due to surface tension is less than 2% of the variation in bubble pressure due to inertial effects and is therefore negligible. Viscous stresses at the bubble and droplet surfaces are neglected. Equation (11) also accounts for differing densities in the droplet and the surrounding liquid.

$$0 = \left(P_b - P_\infty\right) - \frac{2\sigma}{R_b} + \frac{F(t)^2}{2}\left(\frac{\rho_d}{R_b^4} + \frac{\rho_c - \rho_d}{R_d^4}\right) + \frac{dF(t)}{dt}\left(-\frac{\rho_d}{R_b} + \frac{\rho_d - \rho_c}{R_d}\right) \tag{11}$$

At any given time, the pressure in the bubble is determined by the equation of state of the vapor in the bubble. Therefore, Eq. (11) may be used to find the evolution of F(t) over time. This expression of the momentum equation in terms of the source strength is adopted because it simplifies the numerical solution of the balance equations. In the limit as $R_b/R_d \rightarrow 0$, Eq. (11) is equivalent to the Rayleigh equation.

3.2.Energy balance

The energy balance equation in the liquid is,

$$\rho c \frac{\partial T}{\partial t} + \rho c u \frac{\partial T}{\partial r} = \frac{k}{r^2}\frac{\partial}{\partial r}\left(r^2 \frac{\partial T}{\partial r}\right). \tag{12}$$

The temperature is assumed to be uniform inside the vapor bubble, where the vapor is assumed to behave as an ideal gas. During the first time domain it is assumed that the vapor in the bubble is saturated. The saturation pressure and temperature are linked by the Clausius-Clapeyron equation, assuming that the latent heat of vaporization is constant,

$$\frac{P_{sat}}{P_{sat,0}} = \exp\left[\frac{i_{fg}}{R_s}\left(\frac{1}{T_{sat,0}} - \frac{1}{T_{sat}}\right)\right]. \tag{13}$$

After the droplet has completely evaporated, the temperature in the bubble is determined using the energy balance applied to the bubble, including the work done by the expanding bubble and heat diffusion to the bubble surface through the surrounding liquid,

$$\frac{dT_b}{dt} = \frac{4\pi R_b^2}{m_b c_{v,b}}\left(k\frac{\partial T}{\partial r}\bigg|_{r=R_b} - P_b\frac{dR_b}{dt}\right). \tag{14}$$

During the first time domain the mass of vapor in the bubble increases due to evaporation according to,

$$\frac{dm_b}{dt} = \frac{4\pi R_b^2 k_d}{i_{fg}}\frac{\partial T}{\partial r}\bigg|_{r=R_b}. \tag{15}$$

Evaporation at the bubble surface also results in a relative velocity between the bubble surface and the liquid adjacent to the surface given by,

$$\frac{dR_b}{dt} - u\big|_{r=R_b} = \frac{1}{4\pi R_b^2 \rho_d}\frac{dm_b}{dt}. \tag{16}$$

A summary of the variables, initial and boundary conditions, and governing equations is given in Table 1. Two sets of governing equations are given. The first set applies to the first time domain in which evaporation occurs, while the second applies when the droplet is completely evaporated and no phase change occurs.

3.3. Initial and boundary conditions

In all simulations the bubble begins at rest with an initial radius 0.1 percent larger than the critical radius, Eq. (3). The initial temperature is uniform and equal to the ambient temperature. The ambient temperature and pressure are held constant throughout each simulation. Simulations are performed at different ambient temperatures, while in all cases the ambient pressure is held at one atmosphere.

4. Solution method

The simulations represent the temperature profile in the liquid around the bubble by a one-dimensional array of nodes, the first of which is located at the surface of the bubble. The first node also represents the temperature inside the bubble itself; it is assumed that there is no temperature jump across the bubble surface. The last node has temperature fixed at the ambient temperature. Simulations are performed with a total of sixty nodes that are spaced to span a distance of 40 μm from the bubble surface. Using an approach similar to that of Lee and Merte [4], the nodes are clustered near the bubble surface according to,

$$r_j = R_b + (40\,\mu\text{m})\left(\frac{j}{N-1}\right)^2, \tag{17}$$

where j is the node number, $0 \le j \le N\text{-}1$. As the simulation progresses, the nodes move outward with uniform velocity equal to that of the bubble surface. The spacing between nodes therefore remains constant, and the droplet surface moves relative to the nodes as the droplet evaporates.

The equations are solved by an iterative, fully implicit method. Care is taken in defining k, and ρc in each term of the discretized form of Eq. (12) for nodes adjacent to the boundary between the droplet and surrounding liquid. The initial time step size is typically set to 1 ns and is allowed to increase somewhat as the simulation progresses. The droplets typically take between 10 and 100 μs to boil, so simulation durations are between 100 μs and 1 ms.

5. Results

5.1. Conditions

A series of simulations is performed for various combinations of fluids and for a range of droplet sizes and degrees of superheat. Droplet radii are chosen in the range $2 \leq R_d \leq 15$ μm, which are typical of emulsions used in heat transfer research [3,23,24]. Three combinations of fluids are simulated. Droplets of water in mineral oil are simulated to investigate configurations in which the droplet liquid has much higher thermal conductivity than the surrounding liquid. For this combination of fluids superheats of 40 and 80 °C are considered, corresponding to temperatures for which boiling of water-in-oil emulsions is observed experimentally [23].

Simulations are performed with droplets of two liquids, pentane and FC-72, suspended in water. Pentane is typical of light hydrocarbons that have little or no solubility in water and are used in emulsion boiling research [24]. FC-72 is a 3M^{TM} Fluorinert^{TM} electronic liquid that has properties similar to refrigerants such as R-113 and is taken as typical of heat transfer liquids. In these cases the surrounding liquid has higher thermal conductivity and specific heat than the droplet. For these configurations smaller degrees of superheat, 20 to 60 °C, are considered, which also correspond to temperatures at which boiling of oil-in-water emulsions is observed [24]. For all three pairs of fluids, fluid properties are evaluated at the saturation temperature of the more volatile liquid, and properties are assumed to be constant. In all cases the ambient pressure is equal to one atmosphere.

5.2. Initial bubble growth

The initial behavior of the vapor bubble is qualitatively similar to that observed by Lee and Merte [4]. The initial vapor bubble radius is very close to the critical radius so the early motion of the vapor bubble interface is gradual. As the pressure jump due to surface tension decreases, the bubble accelerates outward and the vapor bubble growth enters the inertia dominated phase. As Fig. 2 illustrates, the bubble radius grows at constant rate in the inertia dominated phase as expected. What is novel is that the rate of expansion of the bubble depends on the droplet size as well. Equation (11) shows that a difference in density between the droplet liquid and the surrounding liquid can impact the rate of growth of the bubble, but only when the bubble and droplet radii are of similar magnitude. When $R_b << R_d$ the inertial effects of any difference in density is negligible. Therefore, for water in mineral oil ($\rho_d/\rho_c = 1.17$) the rate of expansion is nearly independent of the droplet size,

while for pentane in water ($\rho_d/\rho_c = 0.614$) the rate of expansion is significantly greater in larger droplets. For FC-72 in water ($\rho_d/\rho_c = 1.63$) the opposite trend is observed (Figs. 2(a) – (c)).

5.3. Final bubble growth

After the initial inertia dominated growth, bubble growth approaches the analytical solution of Mikic et al. [1] until the droplet is mostly evaporated (Figures 3-5). For water in oil and FC-72 in water (fluid combinations for which $\rho_d > \rho_c$) the simulated bubble growth is generally faster than predicted by Eq. (2), while the opposite is true for pentane in water ($\rho_d < \rho_c$). This result is explained by the deviation in the rate of bubble growth during the momentum dominated growth described in the previous section. The simulated bubble growth also tends to run faster than Eq. (2) for larger ΔT. This discrepancy is most likely due to the relation used in this study for the saturation pressure (Eq. 13) which results in a larger initial driving pressure than the relation used by Mikic et al. [1].

As the bubble continues to expand, the layer of droplet liquid surrounding the bubble becomes thinner and eventually evaporates completely. Therefore the thermal boundary layer around the bubble necessarily grows into the liquid that surrounds the droplet. For the water in oil case the oil has lower thermal conductivity, specific heat, and density than the water. All three factors contribute to reducing the rate at which enthalpy is conducted to the bubble surface, which reduces the rate of bubble expansion in the later stages of boiling. For water in oil, the thermal properties of the oil begin to influence the rate of bubble expansion when the bubble reaches approximately one third of its equilibrium radius. For pentane in water and FC-72 in water, the surrounding liquid has much higher thermal conductivity and higher specific heat than the droplet liquid, so the bubble accelerates near the end of the boiling process.

The influence of the properties of the surrounding liquid on the final bubble growth rate is similar to that reported by Avedisian [17]. In the present simulations, dependence on droplet size and degree of superheat is also observed. For all combinations of fluids considered here, these effects at the end of the boiling process are most pronounced for larger droplets and for lower ΔT. The model of Mikic et al. [1] shows that thermal diffusion dominated growth occurs later in the boiling process, so the dependence on

droplet size is expected. Equation (2) also shows that the region of inertia dominated growth grows with increasing ΔT.

5.4. Bubble oscillation

Eventually the bubble must come to rest at its equilibrium radius. Ignoring surface tension this radius is,

$$R_{b,0} = R_{d,0}\left(\frac{\rho_d R_s T_\infty}{P_\infty}\right)^{1/3}. \tag{18}$$

However, when the droplet completely evaporates the liquid around the bubble still has considerable velocity and so the bubble oscillates for some time. The oscillations decay as a result of thermal and acoustic damping [25]. These simulations are not expected to accurately predict the decay of the oscillations because acoustic damping, which depends on the compressibility of the liquid, is not modeled. Neglecting surface tension, small-amplitude oscillations of a spherical vapor bubble are sinusoidal at the Minnaert frequency [26],

$$f_M = \frac{1}{2\pi R_{b,0}}\sqrt{\frac{3\kappa P_\infty}{\rho_c}}. \tag{19}$$

For an isothermal bubble the polytropic coefficient $\kappa = 1$, and for an adiabatic bubble $\kappa = \gamma$. When heat transfer between the bubble and surrounding liquid occurs, κ is expected to fall between these two extremes [25].

As Fig. (6) illustrates, the oscillations of the smaller water vapor bubbles in this study are neither small amplitude nor precisely sinusoidal, and therefore the analytical solutions for small oscillations are not expected to be precisely correct. For all three combinations of fluids, the frequency of oscillation falls close to the Minnaert frequency for an isothermal bubble. The polytropic coefficient varies from a minimum of 0.95 for $R_d = 5$ μm in the

pentane in water case, to a maximum of 1.06 for R_d = 2 μm in the water in oil case, suggesting that the bubble is close to isothermal during oscillations.

Figure (6) also shows that the influence of droplet size on the magnitude of the bubble oscillations is much more significant for the water in oil case than for the pentane and FC-72 in water cases. This behavior is a result of the deceleration or acceleration of the bubble expansion when the droplet is mostly evaporated, as discussed in the previous section. The high thermal conductivity of water also results in much faster decrease in the magnitude of the oscillations due to thermal damping than in the water in oil case.

5.5. Bubble temperature variation

Figures 7 and 8 show the evolution of the bubble temperature over time for the water in oil and FC-72 in water cases. Figure 7 illustrates the decrease in bubble temperature during the early expansion of the bubble. In all cases the initial decrease in bubble temperature is nearly independent of the droplet radius, which is in harmony with the observation that the initial bubble expansion is also nearly independent of the droplet radius. Figure 7(a) shows that for the smaller water droplets in oil, there is a second stage of rapid cooling of the bubble that occurs after the initial expansion begins. This behavior is a result of the thermal boundary layer growing into the oil around the water droplet. As discussed in Section 5.3, as this occurs the rate of heat transfer to the bubble surface decreases. The rate of evaporation therefore decreases, but the inertia of the surrounding liquid prevents the rate of expansion of the bubble from changing instantly. Therefore the specific volume of the vapor in the bubble rises and the temperature decreases. The FC-72 droplet in water has the opposite behavior, wherein the temperature in the bubble begins to rise shortly before the droplet evaporates completely as the remaining layer of FC-72 grows thin.

Figure 8 shows the variation in bubble temperature during the entire boiling process and the first few oscillations of the bubble. Figure 8(a) shows that only for the largest water droplet in oil does the bubble temperature ever reach T_{sat}, and thus experience purely thermal diffusion limited growth. The figure also shows that the bubbles are indeed close to isothermal when oscillating, as the results discussed in the preceding section implied. The rather sharp changes in the FC-72 bubble temperature (Figure 8b) occur near the minimum radius in each oscillation and are caused by FC-72 vapor briefly becoming

saturated at that point in the oscillation. A small amount of FC-72 condenses onto the surface of the bubble, and because FC-72 has poor thermal conductivity, the bubble becomes somewhat insulated. As the bubble expands in the next cycle of oscillation the FC-72 evaporates again.

This intermittent re-condensation of the droplet liquid is, perhaps, less physically realistic than the other results. It seems plausible that because the time during which the FC-72 is saturated is so small, it may remain a subcooled vapor rather than condensing at the bubble surface. To investigate the significance of re-condensation a series of simulations was performed for FC-72 droplets in water in which condensation is not allowed after the initial vaporization of the droplet. The resulting oscillations of the bubble are not significantly different from the simulations in which condensation occurs. As expected the variation of the bubble temperature is diminished. The frequency of oscillation of the bubble and the rate of thermal damping of the oscillations are both slightly lower.

5.6. Comparison with the Kwak et al. model

The model developed by Kwak et al. [21] is also applied to the bubbles simulated in this study. Because their model only describes oscillating bubbles, the initial conditions for numerical calculations using Eq. (4-8) are taken from the results of the simulations performed for this study at the time when the droplet evaporates completely. The initial thermal boundary layer thickness is set so that the initial heat transfer rate to the bubble is the same as the rate predicted by this study. To ensure that the boundary layer thickness remains small compared to the bubble radius it is necessary to increase the temperature range to $|T_b - T_\infty| < 1°C$ for which $d\delta/dt = 0$. It is not surprising that this more severe restriction on Eq. (8) is necessary, as the Kwak et al. model was developed for much larger bubbles.

Figure 9 compares the results of this study to simulations performed using the Kwak et al. model for the oscillating bubble that results from the boiling of a droplet of FC-72 in water with R_d = 15 μm and ΔT = 40 °C. As Fig. (9a) illustrates, the two models are in very close agreement regarding the frequency and initial amplitude of the oscillations. However, the Kwak et al. model predicts significantly larger variation in the bubble temperature, and

the variation increases with time as the thermal boundary layer grows (Fig. 9b). The most likely reason for these discrepancies is the assumption by Kwak et al. of a quadratic temperature profile in the boundary layer. As Fig. (9c) illustrates, the model developed in this study predicts that the temperature profile in the boundary layer can become complex. The shape of the temperature profile predicted by this study at $t = 40$ μs contains the entire history of the boiling droplet including heat transfer to the droplet during the boiling process and bubble expansion ($0 < t < 24$ μs), heat transfer from the bubble during its subsequent contraction ($24 < t < 38$ μs), and finally heat transfer to the bubble again as it begins to expand again (38 μs $< t$). Any model that assumes a temperature profile in the boundary layer cannot capture this behavior.

6. Conclusions

Boiling of very small superheated droplets and oscillation of the resulting bubbles is simulated using a one-dimensional model incorporating the momentum and energy equations. The model is suitable for boiling at moderate superheat where the bubble does not exhibit instability [18]. Results indicate that initial vapor bubble growth is well predicted by classical theory based on the properties of the droplet alone. The final growth rate of the bubble is significantly affected by the properties of the liquid around the droplet, similar to the findings of Avedisian [17]. The final rate of bubble expansion increases when the liquid around the droplet has higher thermal conductivity, density, and specific heat than the droplet. The final rate of expansion is reduced when the opposite is true. The present simulations show that this effect is more pronounced for larger droplets and also leads to an increase or decrease, respectively, in the magnitude of the oscillations experienced by the bubble after evaporation of the droplet is complete. The temperature of the bubble is nearly constant during the subsequent oscillations, and although the magnitude of the oscillations can be large, the frequency of oscillation is close to the expected frequency for an isothermal bubble undergoing small-amplitude oscillations.

The results of this study are compared to an earlier numerical model by Kwak et al. [21] of oscillating bubbles that does not model heat conduction in the boundary layer in detail. The models are generally in close agreement. However, the Kwak et al. model fails to

capture the complex temperature profiles that develop in the boundary layer and predicts larger temperature variation in the oscillating bubble.

References

[1] B. B. Mikic, W. M. Rohsenow, P. Griffith, “On bubble growth rates,” International Journal of Heat and Mass Transfer, **13**(4) (1970), pp. 657-666.

[2] S. Sideman, Y. Taitel, “Direct-contact heat transfer with change of phase: Evaporation of drops in an immiscible liquid medium,” International Journal of Heat and Mass Transfer, **7**(11) (1964), pp. 1273-1289.

[3] N. V. Bulanov, B. M. Gasanov, “Peculiarities of boiling of emulsions with a low-boiling disperse phase,” International Journal of Heat and Mass Transfer, **51**(7-8) (2008), pp. 1628-1632.

[4] H. S. Lee, H. Merte, “Spherical vapor bubble growth in uniformly superheated liquids,” International Journal of Heat and Mass Transfer, **39**(12) (1996), pp. 2427-2447.

[5] M. S. Plesset, S. A. Zwick, “The growth of vapor bubbles in superheated liquids,” Journal of Applied Physics, **25**(4) (1954), pp. 493-500.

[6] Rayleigh, “On the pressure developed in a liquid during the collapse of a spherical cavity,” London, Edinburgh, and Dublin Philosophical Magazine and Journal of Science, **34** (sixth series) (1917), pp. 94-98.

[7] T. G. Theofanous, P. D. Patel, “Universal relations for bubble growth,” International Journal of Heat and Mass Transfer, **19**(4) (1976), pp. 425-429.

[8] Y.-C. Lien, “Bubble Growth Rates at Reduced Pressure,” Ph.D. Thesis, Massachusetts Institute of Technology, Cambridge, Massachusetts, 1969.

[9] Y. Tochitani, Y. H. Mori, K. Komotori, “Vaporization of single liquid drops in an immiscible liquid part 1: Forms and motions of vaporizing drops,” Wärme- und Stoffübertragung, **10** (1977), p. 51-59.

[10] Y. Tochitani, T. Nakagawa, Y. H. Mori, K. Komotori, “Vaporization of single liquid drops in an immiscible liquid part 2: Heat transfer characteristics,” Wärme- und Stoffübertragung, **10** (1977), p. 71-79.

[11] P. Battya, V. R. Raghavan, K. N. Seetharamu, “Parametric studies on direct contact evaporation of a drop in an immiscible liquid,” International Journal of Heat and Mass Transfer, **27**(2) (1984), pp. 263-272.

[12] S. T. Vuong, S. S. Sadhal, "Growth and translation of a liquid-vapour compound drop in a second liquid, Part 1: Fluid mechanics," Journal of Fluid Mechanics, **209** (1989), pp. 617-637.

[13] S. T. Vuong, S. S. Sadhal, "Growth and translation of a liquid-vapour compound drop in a second liquid, Part 2: Heat transfer," Journal of Fluid Mechanics, **209** (1989), pp. 639-660.

[14] G. K. Raina, P. D. Grover, "Direct contact heat transfer with change of phase: Theoretical model incorporating sloshing effects," AIChE Journal, **31**(3) (1985), pp. 507-510.

[15] H. B. Mahood, "Direct-contact heat transfer of a single volatile liquid drop evaporation in an immiscible liquid," Desalination, **222** (2008), pp. 656-665.

[16] M. G. Wohak, H. Beer, "Numerical simulation of direct-contact evaporation of a drop rising in a hot, less volatile immiscible liquid of higher density – possibilities and limits of the SOLA-VOF/CSF algorithm," Numerical Heat Transfer, Part A: Applications, **33** (1998), pp. 561-582.

[17] C. T. Avedisian, "Bubble growth in superheated liquid droplets," in: N. P. Cheremisinoff (ed), Encyclopedia of Fluid Mechanics, Volume 3, Gulf Publishing, Houston, 1986, pp. 130-190.

[18] J. E. Shepherd, B. Sturtevant, "Rapid evaporation at the superheat limit," Journal of Fluid Mechanics, **121** (1982), pp. 379-402.

[19] H. S. Lee, H. Merte, "Explosive vapor bubble growth in uniformly superheated liquids: R-113 and mercury," International Journal of Heat and Mass Transfer, **48**(13) (2005), pp. 2593-2600.

[20] D. Frost, B. Sturtevant, "Effects of ambient pressure on the instability of a liquid boiling explosively at the superheat limit," Journal of Heat Transfer, **108**(2) (1986), pp. 418-424.

[21] H. Y. Kwak, S. D. Oh, C. H. Park, "Bubble dynamics on the evolving bubble formed from the droplet at the superheat limit," International Journal of Heat and Mass Transfer, **38**(9) (1995), pp. 1709-1718.

[22] H. C. Park, K. T. Byun, H. Y. Kwak, "Explosive boiling of liquid droplets at their superheat limits," Chemical Engineering Science, **60** (2005), pp. 1809-1821.
[23] Y. H. Mori, E. Inui, K. Komotori, "Pool boiling heat transfer to emulsions," Journal of Heat Transfer, **100**(4) (1978), pp. 613-617.
[24] N. V. Bulanov, B. M. Gasanov, E. A. Turchaninova, "Results of experimental investigation of heat transfer with emulsions with low-boiling disperse phase," High Temperature, **44**(2) (2006), pp. 267-282.
[25] M. S. Plesset, A. Prosperetti, "Bubble dynamics and cavitation," Annual Review of Fluid Mechanics, **9** (1977), pp. 148-185.
[26] C. E. Brennen, Cavitation and Bubble Dynamics, New York: Oxford University Press, 1995, pp. 113-118.

Table

Table 1. Quantities and formulas in the one-dimensional model of a boiling droplet.

Quantity	**Initial / boundary conditions**	**Governing equations**	
		with phase change (1^{st} time domain)	**without phase change (2^{nd} time domain)**
$T(r,t)$	$T(r,0) = T_\infty$ $T(R_b,t) = T_b$	Eq. (12)	Eq. (12)
$F(t)$	$F(0) = 0$	Eq. (11)	Eq. (11)
$m_b(t)$	$m_b(0) = \frac{4}{3}\pi R_b^3(0)\frac{P_\infty}{RT_\infty}$	Eq. (15)	$m_b = m_d$
$R_b(t)$	$R_b(0) = \frac{1.001 \cdot 2\sigma}{P_{sat}(T_\infty) - P_\infty}$	Eq. (16)	$\frac{dR_b}{dt} = u\big\|_{r=R_b}$
$R_d(t)$	N/A	$R_d = \left(R_b^3 + \frac{m_d - m_b}{4/3\pi\rho_d}\right)^{1/3}$	$R_d = R_b$
$T_b(t)$	$T_b(0) = T_\infty$	$T_b = T_{sat}$	Eq. (14)
$P_b(t)$	N/A	$P_b = P_{sat} = \rho R T_b$	$P_b = \rho R T_b$

Figure captions

Figure 1. Pressure and temperature fields in and around vapor bubbles for (a) inertia dominated growth and (b) thermal diffusion dominated growth.

Figure 2. Initial bubble growth for (a) water droplets in oil with $\Delta T = 40$ °C, (b) pentane droplets in water with $\Delta T = 20$ °C, and (c) FC-72 droplets in water with $\Delta T = 20$ °C.

Figure 3. Bubble growth for water droplets suspended in mineral oil with (a) $\Delta T = 40$ °C and (b) $\Delta T = 80$ °C. Equation (2) calculated using properties of water.

Figure 4. Bubble growth for pentane droplets suspended in water with (a) $\Delta T = 20$ °C and (b) $\Delta T = 60$ °C. Equation (2) calculated using properties of pentane.

Figure 5. Bubble growth for FC-72 droplets suspended in water with (a) $\Delta T = 20$ °C and (b) $\Delta T = 40$ °C. Equation (2) calculated using properties of FC-72.

Figure 6. Oscillation of (a) water vapor bubble in mineral oil, $\Delta T = 40$ °C, (b) pentane vapor bubble in water, $\Delta T = 20$ °C, and (c) FC-72 vapor bubble in water, $\Delta T = 20$ °C.

Figure 7. Temperature at bubble surface during initial expansion for (a) water in oil, $\Delta T = 40$ °C and (b) FC-72 in water, $\Delta T = 20$ °C.

Figure 8. Temperature at bubble surface for (a) water in oil, $\Delta T = 40$ °C and (b) FC-72 in water, $\Delta T = 20$ °C.

Figure 9. Predictions of (a) radius and (b) temperature for oscillating FC-72 vapor bubble in water, and (c) boundary layer temperature profile, $\Delta T = 40$ °C and $R_d = 15$ μm.

Figures

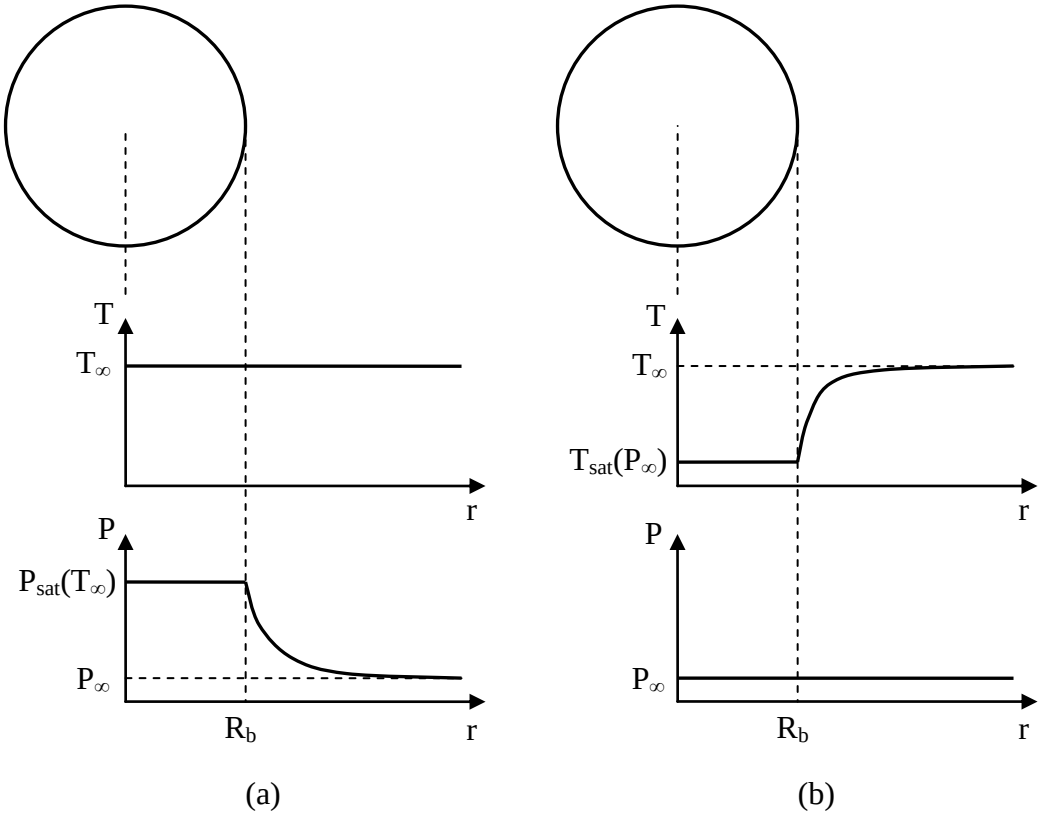

Figure 1. Pressure and temperature fields in and around vapor bubbles for (a) inertia dominated growth and (b) thermal diffusion dominated growth.

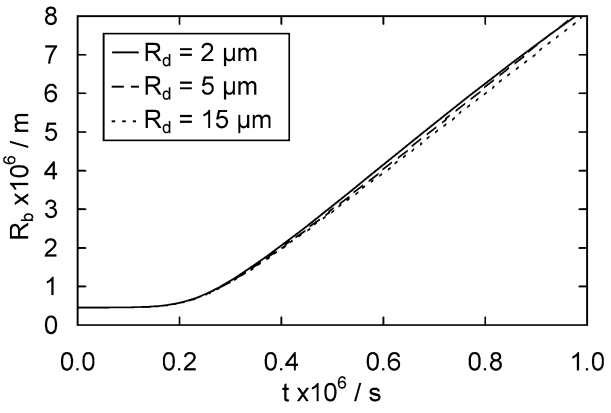

(a)

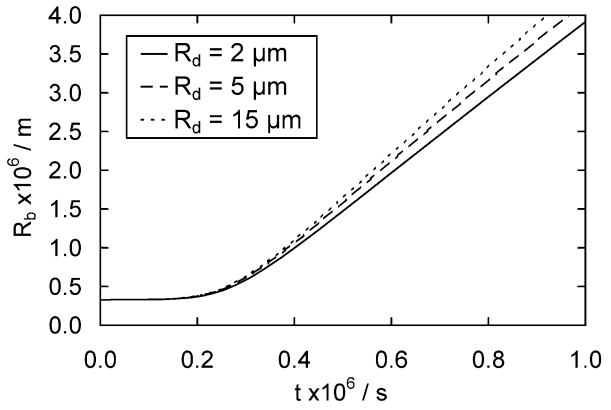

(b)

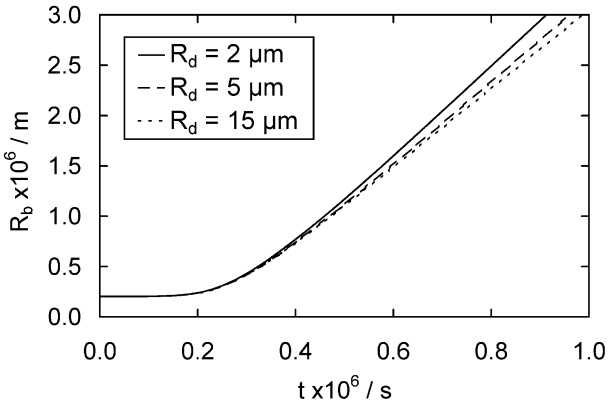

(c)

Figure 2. Initial bubble growth for (a) water droplets in oil with $\Delta T = 40$ °C, (b) pentane droplets in water with $\Delta T = 20$ °C, and (c) FC-72 droplets in water with $\Delta T = 20$ °C.

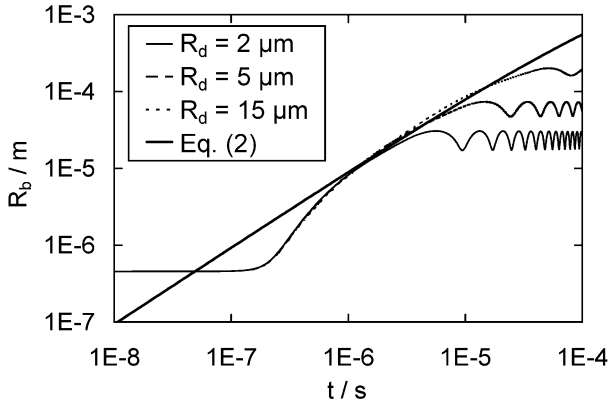

(a)

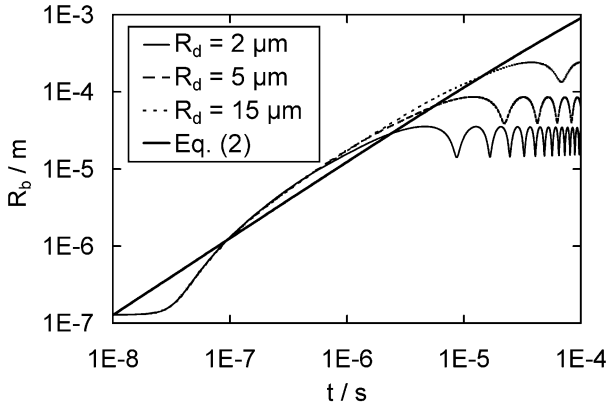

(b)

Figure 3. Bubble growth for water droplets suspended in mineral oil with (a) $\Delta T = 40$ °C and (b) $\Delta T = 80$ °C. Equation (2) calculated using properties of water.

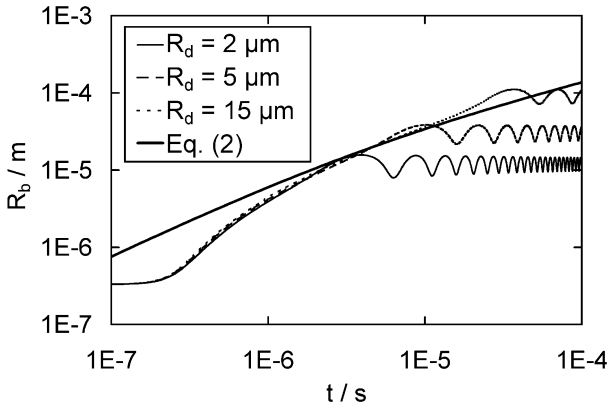

(a)

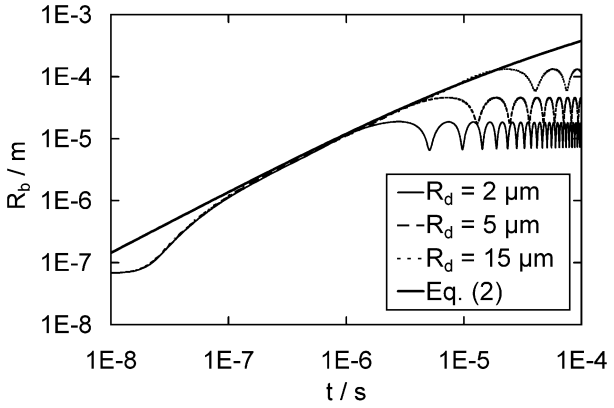

(b)

Figure 4. Bubble growth for pentane droplets suspended in water with (a) $\Delta T = 20$ °C and (b) $\Delta T = 60$ °C. Equation (2) calculated using properties of pentane.

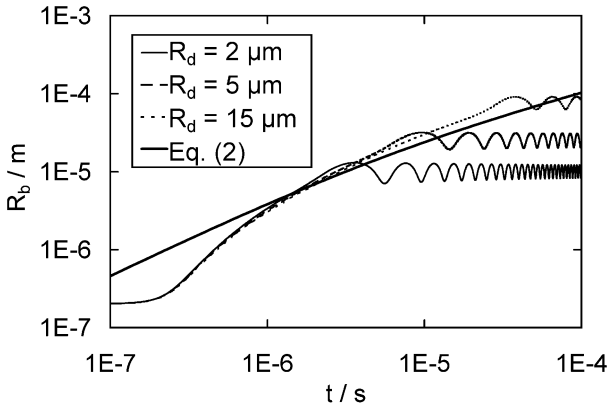

(a)

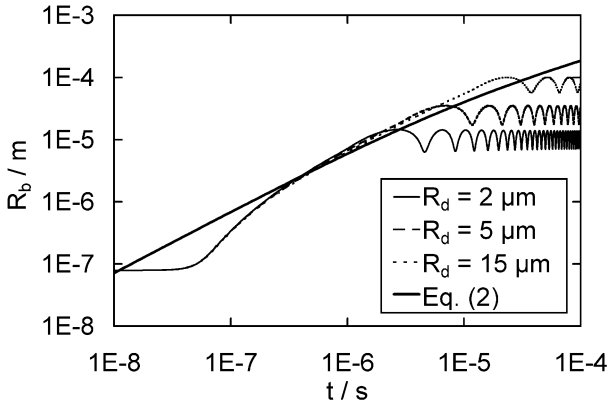

(b)

Figure 5. Bubble growth for FC-72 droplets suspended in water with (a) $\Delta T = 20$ °C and (b) $\Delta T = 40$ °C. Equation (2) calculated using properties of FC-72.

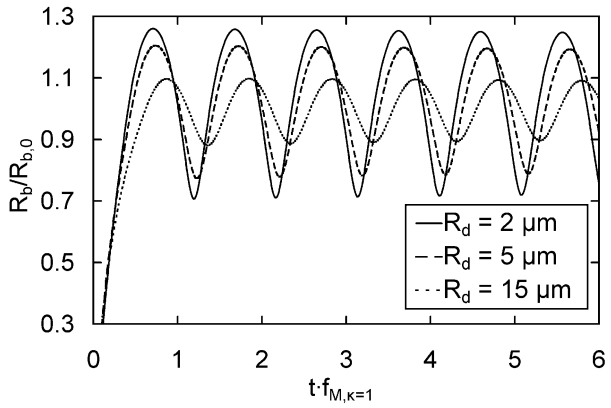

(a)

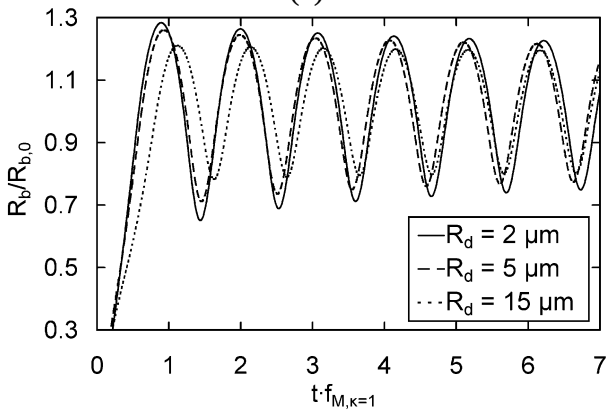

(b)

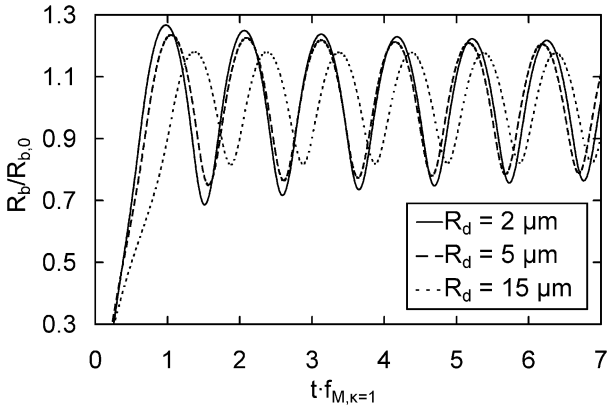

(c)

Figure 6. Oscillation of (a) water vapor bubble in mineral oil, $\Delta T = 40$ °C, (b) pentane vapor bubble in water, $\Delta T = 20$ °C, and (c) FC-72 vapor bubble in water, $\Delta T = 20$ °C.

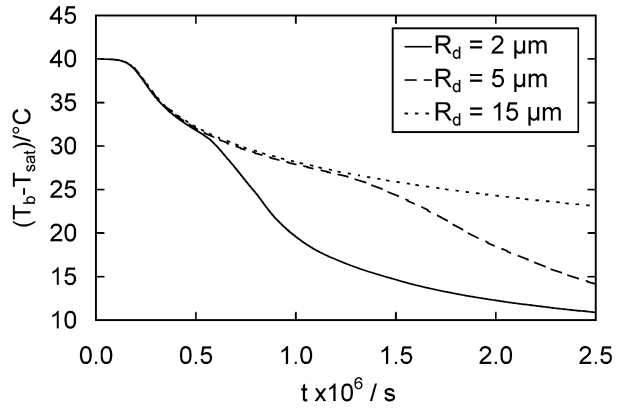

(a)

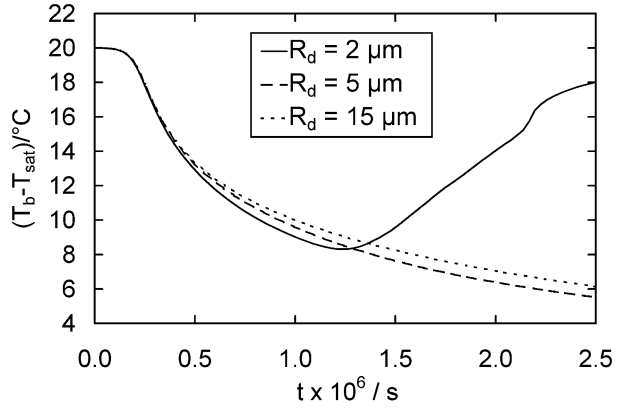

(b)

Figure 7. Temperature at bubble surface during initial expansion for (a) water in oil, ΔT = 40 °C and (b) FC-72 in water, ΔT = 20 °C.

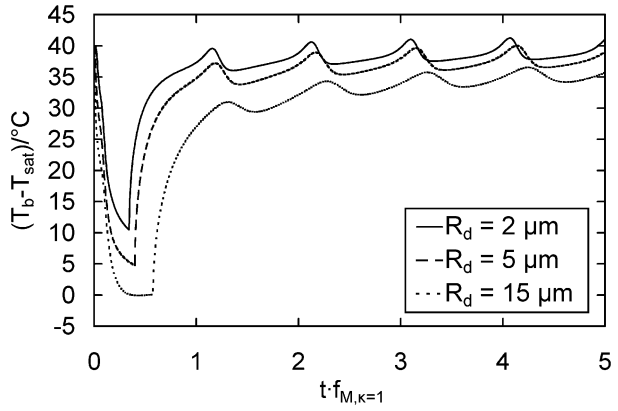

(a)

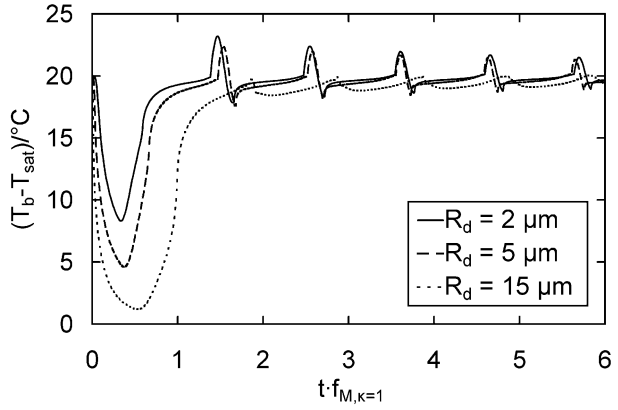

(b)

Figure 8. Temperature at bubble surface for (a) water in oil, $\Delta T = 40$ °C and (b) FC-72 in water, $\Delta T = 20$ °C.

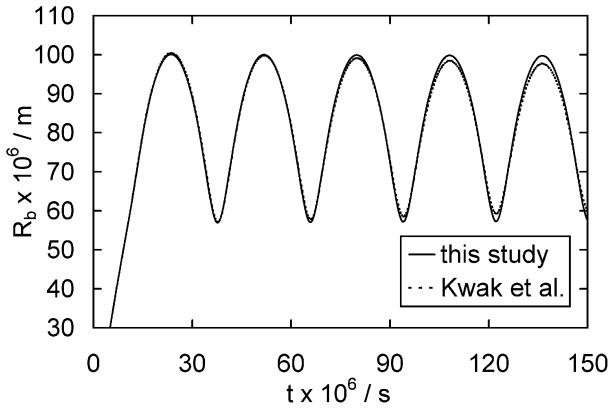

(a)

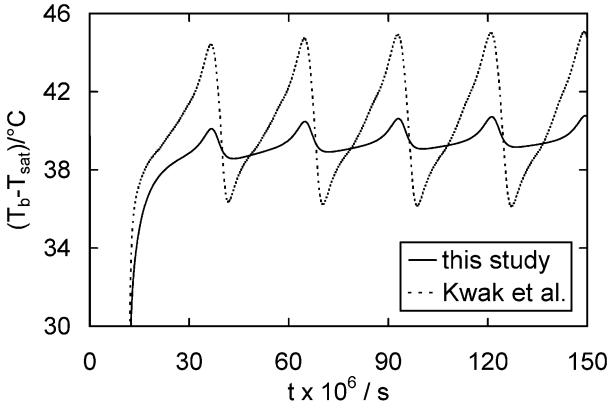

(b)

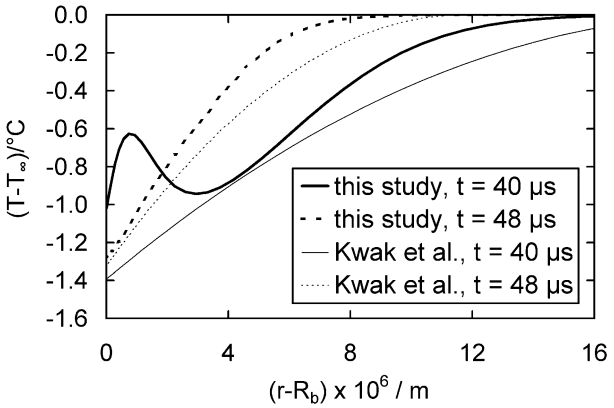

(c)

Figure 9. Predictions of (a) radius and (b) temperature for oscillating FC-72 vapor bubble in water, and (c) boundary layer temperature profile, $\Delta T = 40$ °C and $R_d = 15$ μm.